Horizontal and vertical thermospheric cross-wind from GOCE linear and angular accelerations

T. Visser[a,*], G. March[a], E. Doornbos[a], C. de Visser[a], P. Visser[a]

[a] *Delft University of Technology, Faculty of Aerospace Engineering, Kluyverweg 1, 2629HS Delft, The Netherlands.*

Abstract

Thermospheric wind measurements obtained from linear accelerations of the Gravity field and steady-state Ocean Circulation Explorer (GOCE) show discrepancies when compared to ground-based measurements. In this paper the cross-wind is derived from both the linear and the angular accelerations using a newly developed iterative algorithm. The two resulting data sets are compared to test the validity of the GOCE data and identify possible explanations for the discrepancies with other thermospheric data. In general the difference is found to be less than 50 m/s vertically (after high-pass filtering) and 100 m/s horizontally. The sensitivity analysis reveals that continuous thrusting is a major source of uncertainty, as are the magnetic properties of the satellite. The energy accommodation coefficient is identified as a particularly promising parameter for improving the consistency of thermopsheric cross-wind data sets in the future.

Keywords: Thermospheric wind, Vertical wind, Gravity Field and steady-state Ocean Circulation Explorer (GOCE), Angular accelerations

1. Introduction

The purpose of this paper is to test the possibility of obtaining in situ horizontal and vertical cross-wind from satellite angular accelerations. We do so by presenting a new algorithm that extracts cross-wind from either linear or angular accelerations (or a combination thereof), and applying it

*Corresponding author

Email address: t.visser-1@tudelft.nl (T. Visser)

to measurements of the Gravity field and steady-state Ocean Circulation Explorer (GOCE). The wind measurements derived from linear and angular accelerations are compared and their sensitivity to model parameters is evaluated.

Although accelerations are an intuitive source for in situ wind observations, it has proven to be difficult to align such measurements with existing knowledge and models, as well as with remote observations such as Fabri-Perot Interferometry (FPI) (Dhadly et al., 2017, 2018). Instead of tuning the aerodynamic model of GOCE to match the other observations directly, we first find a set of model parameters for which the linear and angular acceleration data is internally consistent. This paper serves to quantify what level of accuracy can be expected from this approach, and to identify the most sensitive model parameters.

The concept of simultaneous atmospheric observations using linear and angular motion of satellites was first adopted in the paddlewheel satellite concept (Moe, 1966; Pilinski et al., 2011). For those missions the goal was to measure the absolute thermospheric density. The paddlewheel shape of the satellites ensured that aerodynamic loads would both affect the orbital and the spin motion of the body. In recent years a number of accelerometer missions have been operated, that presented an opportunity to obtain high resolution density data (Bruinsma et al., 2004; Doornbos, 2011; Falin et al., 1981; March et al., 2018; Mehta et al., 2017; Siemes et al., 2016). The availability of cross-track accelerations has subsequently lead to a large amount of horizontal cross-wind data (Cheng et al., 2008; Doornbos et al., 2010; Sutton et al., 2005), while the vertical acceleration was generally deemed too small to obtain reliable wind measurements. Although an attitude-based algorithm has been proposed by Virgili-Llop et al. (2018), all accelerometer-derived wind measurements have so far been obtained from linear accelerations.

In this work we apply the concept of simultaneous observation of linear and angular motion to a new accelerometer-based method of deriving horizontal and vertical thermospheric cross-wind. In short the approach is as follows. The measured accelerations are used to calculate a 'measured' net force and torque acting on the satellite. Models are used to estimate forces and torques caused by solar radiation pressure and the ion thruster, and torques caused by the gravity gradient, magnetic attitude control, and other magnetic equipment in the satellite. These models for disturbance forces and torques are described extensively by Doornbos (2011) and Visser et al. (2018) respectively. The residual force and torque, obtained by subtracting the to-

tal model output from the measurement, is assumed to be aerodynamic. An aerodynamic model is made to match this residue by iteratively changing the direction of the incoming flow. The wind is defined as the difference between this new flow direction and the original aerodynamic velocity. The two resulting wind data sets are aligned by iteratively changing the thruster misalignment angles – the most sensitive parameter in the models – and the vertical acceleration bias.

The algorithm presented in this paper can be applied to any mission for which detailed knowledge is available of either the linear or angular accelerations, or an appropriate combination thereof. It can therefore, in itself, contribute to an increase in the amount of missions deemed suitable for wind estimation. One may for example consider to obtain the angular accelerations from precise attitude measurements, and the forward acceleration from the orbital motion. In the GOCE case the algorithm results in two separate cross-wind data sets, one derived from linear accelerations, the other from angular accelerations. By comparing the two we identify the major error sources in accelerometer derived wind, and quantify their impact on the wind measurements. We formulate recommendations for ground testing campaigns, operations, and documentation of future low-Earth-orbiting, accelerometer-carrying satellite missions to improve the consistency of future wind data sets.

The paper is structured as follows. First in section 2 we present the data sets used as inputs, and highlight the changes that were made to earlier (published) versions of the force and torque models. Then the methodology is presented in section 3. The majority of this section is dedicated to the explanation of the algorithm with which the cross-wind is obtained from residual forces and torques. In section 4 the resulting data sets are presented and compared, and their sensitivity to measurement errors and model parameters is evaluated in section 5. Finally in section 6 conclusions are drawn regarding the consistency of accelerometer-derived cross-wind data, and the value of simultaneous wind estimation from linear and angular accelerations.

2. Preliminaries

The goal of the GOCE mission was to map Earth's gravity field in unprecedented detail. For this mission the satellite was equipped with a gradiometer consisting of six accelerometers positioned on the three principle axes of the satellite body, each measuring the linear acceleration along all three princi-

ple axes. The resulting 18 accelerations can be combined in specific ways to obtain the gravity gradients. By taking different combinations of the individual acceleration measurements, the linear and angular accelerations of the satellite body are found. These are used in this work to derive the in situ thermospheric wind. The low orbit required for the mission results in a large aerodynamic signal. We will show in section 4 that this even allows for vertical wind measurements on the heavily controlled pitch axis.

Even though the aerodynamic signal is large, accurate models of all other major disturbance forces and torques are required. In terms of forces this amounts to modeling the thrust, and solar, Earth albedo, and infrared radiation pressure. The first is provided as part of the housekeeping data in terms of the commanded thrust, which is less erratic than the achieved thrust (Wallace et al., 2011). The latter is derived from the position of the Sun and Earth with respect to the satellite, and using ANGARA force coefficients (Doornbos, 2011; Visser et al., 2018). Other, smaller disturbances, such as the third body gravity of the moon, are neglected. The sum of the models is compared to the 'measured' force, defined as the product of the calibrated linear accelerations and interpolated mass of the satellite.

In terms of the torques a total of five different disturbances are modeled, namely the thruster misalignment, solar, Earth albedo and infrared radiation pressure, gravity gradient, attitude control, and magnetic torques. These models are all described and validated by Visser et al. (2018). The calculation of the 'measured' torque and the aerodynamic model are however slightly different. First, instead of calibrating the EGG_CGA product, the 'measured' torque is calculated entirely from the EGG_GAR angular rate product. The angular acceleration is derived from this product by taking the eight point central difference of the original 1Hz signal. The result is interpolated on a 0.1Hz signal, as are all other data. Second the aerodynamic coefficients are obtained from a new high-fidelity geometric model of GOCE using the SPARTA software. This model is described in detail and compared to other existing models by March et al. (2018). We assume a fully diffusive reflection with energy accommodation 0.93. Third, to completely decouple linear and angular accelerations we use NRLMSISE-00 densities and no wind data or model to calculate the initial aerodynamic torque. Only the payload magnetic dipoles are affected by this change, as they are re-estimated using the new set of models.

Since the publication of the GOCE torque models, the scientific data of the mission has been reprocessed to account for the quadratic calibration term

of the accelerometers (Siemes, 2018). This reprocessing had no significant effect on the measured and modeled forces and torques. Only small changes were found in magnetometer calibration parameters and estimated magnetic dipoles. The reprocessed data is used for all results shown in this paper.

3. Methodology

In this section we present a new algorithm that can be used to derive both horizontal and vertical cross-wind from both linear and angular accelerations. Because torques are more intuitive to work with than angular accelerations, the algorithm is set up to work with forces and torques instead. As there is mathematically no difference between force and torque vectors, any combination of force and torque components can be used as input. In our experience the horizontal cross-wind is observed both in the lateral body force (Y) and the yaw torque (N); the vertical wind affects both the vertical force (Z) and the pitch torque (M); the density primarily affects the longitudinal force (X). In roll (L) the aerodynamic torques are too small to yield a valuable wind or density measurement. In the remainder of this paper we mean by torque-derived wind, wind derived from pitch and yaw torques and longitudinal force (X, M, N).

The residual forces and torques are obtained by reducing the measured forces and torques by modeled disturbances, as discussed in section 2. It was found that when forces and torques are mixed, scaling of the residuals is required to prevent a bias towards the force residual. Therefore the torque residual is multiplied by 10. In the remainder of this section we discuss the algorithm in terms of torques only. The process is exactly the same for forces.

The algorithm is an implementation of the Frank–Wolfe algorithm. Each iteration consists of six steps, as presented in figure 1 and outlined below. It is initialized with the orbital velocity including co-rotation of the atmosphere and densities obtained from NRLMSISE-00.

1. Based on the (initial) aerodynamic velocity $\boldsymbol{V}_i$ the aerodynamic torque is calculated. Both the aerodynamic $\boldsymbol{T}_A$ and residual torque $\boldsymbol{T}_R$ are normalized to $\hat{\boldsymbol{T}}_A$ and $\hat{\boldsymbol{T}}_R$, and the error $\Delta\boldsymbol{T}$ between the two is found.
2. The direction error is converted to an angle μ between the two torques, and the direction vector $\boldsymbol{e}$. The latter is defined as the vector perpendicular to $\hat{\boldsymbol{T}}_A$, tangential to the great circle through $\hat{\boldsymbol{T}}_A$ and $\hat{\boldsymbol{T}}_R$, centered at the center of mass of the satellite.

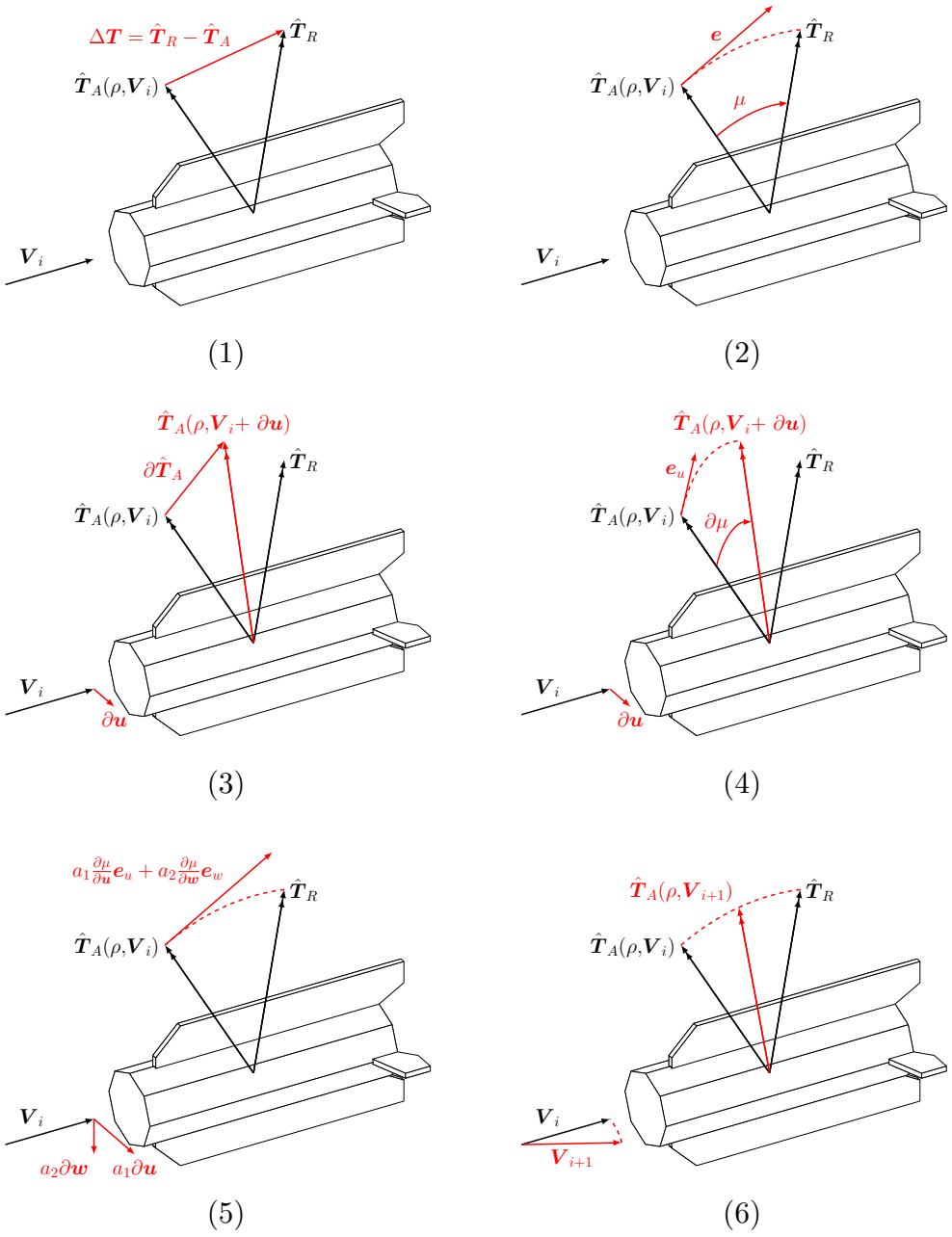

Figure 1: Schematic overview of the six steps of the algorithm to determine the wind from the torque measurements and models. The same algorithm is applied to derive wind from measured and modeled force. Note that direction vectors $\boldsymbol{e}$ and normalized torques (indicated with a hat) are drawn with different lengths to improve the clarity of the figure.

3. Using the Gram-Schmidt method two directions perpendicular to the current aerodynamic velocity are found. Small changes are made to the velocity in those directions (only drawn for $\boldsymbol{u}$ in Fig. 1) and the aerodynamic torque is recalculated and normalized.
4. The changes in aerodynamic torque direction $\partial\hat{\boldsymbol{T}}_A$ due to these velocity variations are decomposed into an angle $\partial\mu$ and the tangential $\boldsymbol{e}_u$ along the great circle through the old and new aerodynamic torque. Dividing the angle increment by the change in velocity we find approximate derivatives of these angles.
5. The derivatives are collected in a Jacobian matrix. Assuming a linear relation, we solve the system

$$\mu\boldsymbol{e} = \left[\begin{array}{cc} \frac{\partial\mu}{\partial\boldsymbol{u}}\boldsymbol{e}_u & \frac{\partial\mu}{\partial\boldsymbol{w}}\boldsymbol{e}_w \end{array} \right] \boldsymbol{a} \tag{1}$$

   for the parameters in $\boldsymbol{a}$ in a weighted least squares sense. The weights are chosen to be the inverse standard deviation of the measured torque components.
6. The update is scaled with a learning rate γ_i before it is applied to the velocity update components $\boldsymbol{u}$ and $\boldsymbol{w}$. The learning rate gradually increases as $\gamma_i = \min\{0.1 + i/10, 0.9\}$. The velocity is normalized to its original magnitude.

The algorithm normally converges in 10 iterations, using a maximum angle error $\max(\mu) < 1''$ as the stopping criterion. The wind is defined as the difference between the final aerodynamic velocity and the initial (orbital plus co-rotation) velocity. After convergence a separate scale factor is estimated for the density at each time instant, minimizing the difference between the aerodynamic and residual torque in a least squares sense.

The total (three-dimensional) wind measurements are rotated from the body frame (in which they are derived) to the local inertial orbit frame. The horizontal cross-wind is thus defined along the orbital angular momentum vector, and the vertical wind along the radial direction. The differences between this frame and the body frame are minimal, except for a rotation of 180 degrees around the longitudinal axis. This ensures that positive vertical wind is upward. Due to the dusk-dawn orbit configuration, positive horizontal wind blows from night to day.

Because the velocity is normalized in every step, any cross-wind will also change the along-track component of the velocity, resulting in an along-track

wind component. These measurements are not considered to be real wind data. The main along-track wind contribution is included in the density measurement, and cannot be uniquely identified based on accelerometer measurements alone. In theory the algorithm could estimate the along-track wind if four or more force and torque components are combined. In practice however the aerodynamic force and torque models are not linearly independent in their response to flow incidence angles.

Applying the above algorithm to the entire GOCE mission, we found a strong bias towards upward wind, and an offset between cross-wind components derived from forces and those derived from torques. From the sensitivity analysis (discussed in detail in section 5) it was concluded that both could be explained by a small adjustment of both the vertical acceleration bias and the thruster misalignment angles. Therefore a second, overarcing iterative algorithm is used to estimate aforementioned parameters. In this Frank–Wolfe implementation the derivatives of the wind components with respect to the vertical acceleration bias and thruster misalingment angles are calculated from a forward difference. The wind is assumed to be linear in these parameters, and the system is solved. Because angles are small in this case, the algorithm converges in one iteration with learning rate 1.

This algorithm is run for each day resulting in the daily estimates plotted in Fig. 2 (after removing a total of 28 outliers). Four linear trends have been estimated for the thrust angles as a function of mean thrust level, in accordance with the documentation (Kolkmeier et al., 2008, see Table 6.6-2). They are plotted in the same figure, and listed in Table 2. The episodes were chosen based on visual inspection of Fig. 2, and constitute the time before and after August 2012 respectively, as well as the months August and November of 2012. These two months deviate from the nominal mission because of significant orbit lowering operations (GOCE Flight Control Team (HSO-OEG), 2014). Although the parameterization is based on the daily mean thrust level, the angles are calculated using the instantaneous thrust in the updated force and torque models.

The daily vertical acceleration bias estimates is plotted alongside the estimates from orbit determination (using the method of Visser and van den IJssel (2016) and the reprocessed GOCE data) in Fig. 3. Note that the orbit-based estimates are more scattered than the wind-based ones. Bias estimates below -46 nm/s^2 and above 10 nm/s^2 are removed before four linear trends in time are estimated. Instead of isolating the November 2012 orbit maneuver, the early part of the mission (before the summer 2010 anomaly

Table 1: Linear parameterizations of the thrust pitch and yaw angles α and β in terms of the thrust level.

	Pitch α [deg, deg/N]		Yaw β [deg, deg/N]	
Time period	Constant	Linear	Constant	Linear
2009-11-01 – 2012-07-31	-2.16	24.22	-0.01	35.14
2012-08-01 – 2012-08-31	-2.24	65.71	0.63	-103.53
2012-09-01 – 2012-10-31[a]	-2.06	9.83	0.09	12.06
2012-11-01 – 2012-12-02	-2.13	25.27	0.34	-12.45
2012-12-03 – 2013-09-30[a]	-2.06	9.83	0.09	12.06

[a] These episodes were merged to find a single parameterization.

Table 2: Linear parameterizations of the wind-derived vertical acceleration bias as a function of time. Time is measured in days since the start of the episode.

Time period	Constant [nm/s^2]	Linear [nm/s^2/day]
2009-11-01 – 2010-07-31	-36.06	-0.0053
2010-08-01 – 2012-07-31	-34.34	0.0036
2012-08-01 – 2012-08-31	-38.46	0.1546
2012-09-01 – 2013-09-30	-30.56	0.0100

(GOCE Flight Control Team (HSO-OEG), 2014)) is treated separately. The spread in the bias is larger for this part of the mission because of low solar activity and the resulting small aerodynamic force and torque, allowing for errors in other models to become more dominant in the derived wind.

Using the linear parameterizations for the thruster angles and the acceleration bias the thrust force and moment and the measured force are recalculated. Then the residual torque and the payload dipole estimates are updated. The updated models serve as inputs to the algorithm described before to obtain the force- and torque-derived cross-wind.

4. Results

A total of four data sets result from the aforementioned approach: horizontal and vertical cross-wind derived from forces or torques. Because force modeling is significantly less complex that torque modeling, we assume that the force-derived wind is correct. This assumption allows us to evaluate the quality of the torque-derived wind.

A complete mission overview of the horizontal wind is plotted in Fig. 4. It shows the dependence of the horizontal wind on the argument of latitude, i.e. the progress through the orbit in degrees starting from the ascending node. The location of the magnetic poles (at 90 deg argument of latitude for the

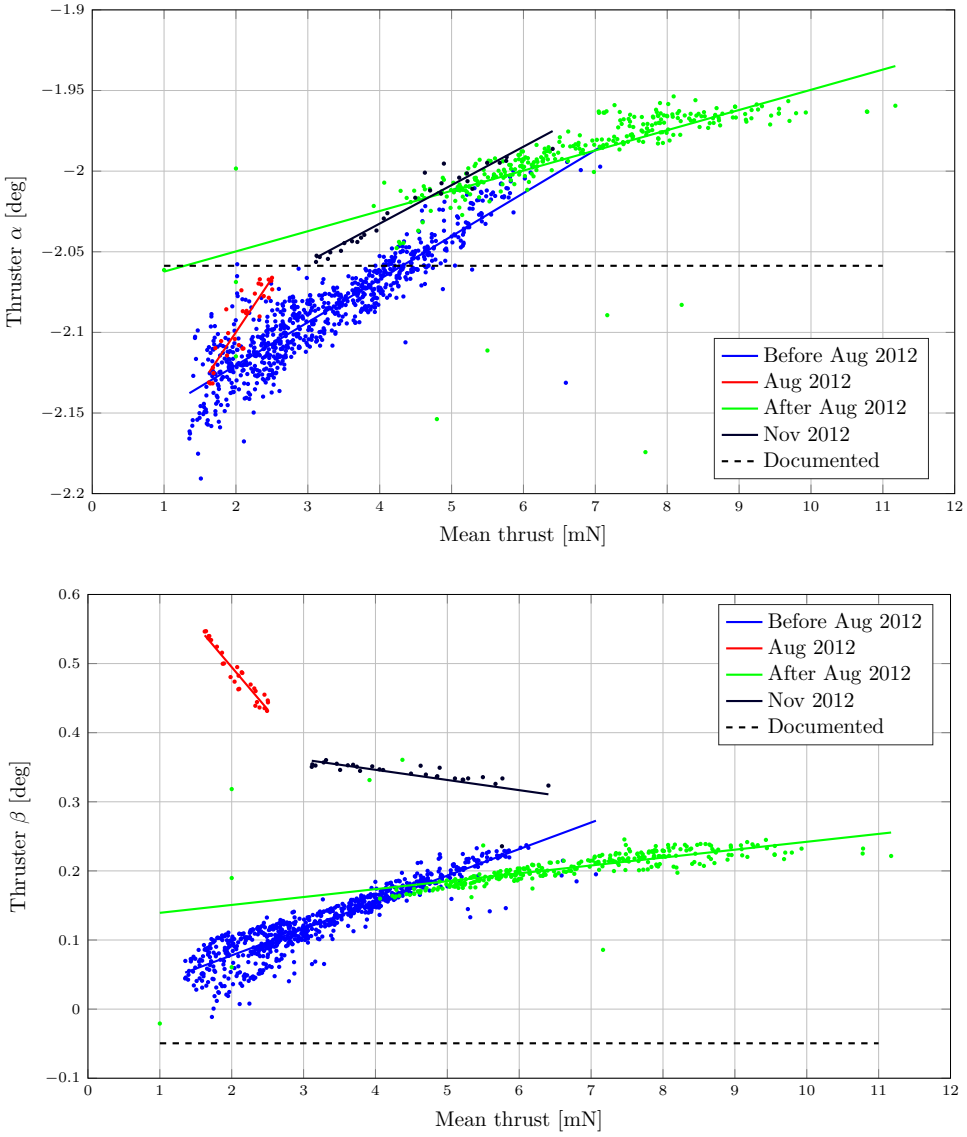

Figure 2: Daily thrust pitch (top) and yaw estimates as a function of daily mean thrust.

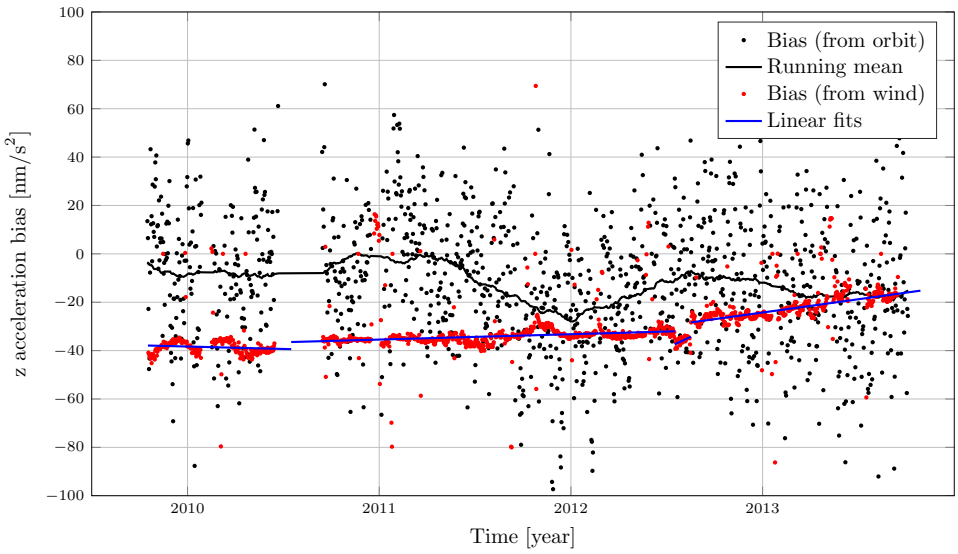

Figure 3: Daily wind-derived z-acceleration bias estimates as a function of time along with the linear parameterizations, compared to orbit-derived biases. Estimates below -42 and above -20 nm/s^2 are considered outliers.

North pole and 270 deg for the South pole) is visible as a region of increased wind and wind reversal. The dominant negative sign of the horizontal wind indicates a net flow from the day to the night side of the Earth, as should be expected. The eclipse transitions are visible in both force- and torque-derived wind because of an overly simplistic eclipse transition model.

The difference between the two data sets, plotted in the bottom panel of Fig. 4, reveals two main trends. First is a difference between the two hemispheres. This trend closely follows the vertical component of the Earth's magnetic field. It could be explained by an electric dipole in the order of 10^{-5} Cm, but no source for a sufficiently large charge has been identified so far. The second trend takes the form of a group of once per year oscillations in argument of latitude. It follows the eclipse pattern observed in the other two panels, implying a relation with the sunlight incidence angle (or: local time). The pattern disappears inside eclipse. This error can be caused by errors in the solar radiation pressure modeling, or by the unmodeled magnetic effect of currents from the solar panels. The difference between the horizontal cross-wind data sets is generally smaller than 100 m/s.

The same overview is plotted for the vertical wind in Fig. 5. The discrep-

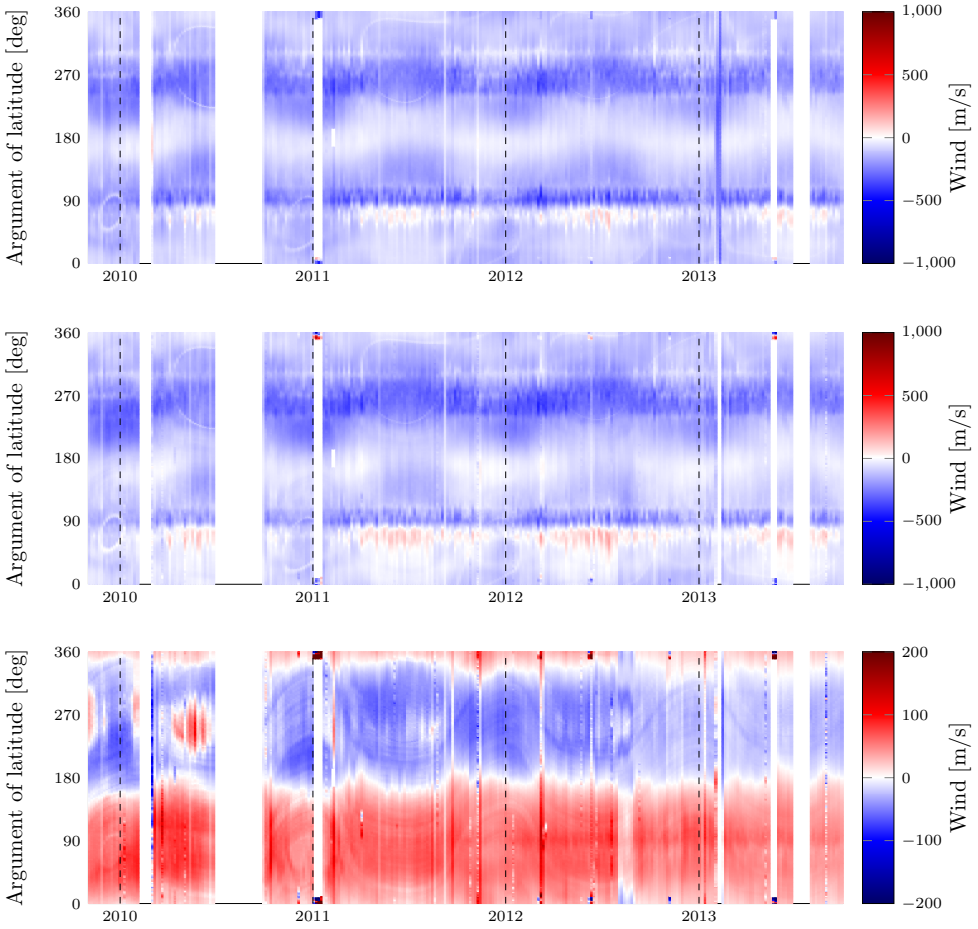

Figure 4: Horizontal wind derived from forces (top) and torques (middle), and the difference between the two, for the full mission.

ancy between these two data sets is significantly larger, as is illustrated by the similarity of the torque-derived data (middle panel) to the difference (bottom panel). The largest errors in the torque-derived wind are found around the South pole (apogee) in local winter, especially early in the mission (at low solar activity); i.e. when density is low. These errors are caused by unmodeled erratic behavior of the thruster at low thrust levels, as reported by Wallace et al. (2011). We also observe a bias in the vertical wind of 30 m/s or less, despite the efforts to remove it using the linear acceleration bias and the thruster misalignment.

As vertical wind is generally characterized by short-lived, small-scale peaks (Innis and Conde, 2002; Smith, 1998), it is worthwhile to compare the two data sets in terms of their high frequencies only. Through trial and error we found that at frequencies above ten times orbital frequency, the two data sets show striking similarities. This is shown in Fig. 6, where the two data sets and their difference are plotted from 11:25 to 11:50 UTC on 17 March 2013, after passing them through a high-pass third-order Butterworth filter rejecting frequencies below ten times the orbital frequency. The difference is reduced to less than 50 m/s, and a strong correlation is revealed between the force- and torque-derived data. We have strong indications that the observed peaks are actual vertical wind measurements, which will be the subject of a separate publication.

5. Sensitivity analysis

As the algorithm output is affected by model parameters and measurement errors, the sensitivity of the wind data is evaluated for both. Uncertainty values are applied as constant positive offsets from the nominal case, except for the accommodation coefficient, which replaces the default value of 0.93. Using the new parameter value the modeled and measured force and torque are calculated anew for March 2013. Note that the affected torque replaces the old version in the notch-filtered residual torque (as per the terminology and methodology used by Visser et al. (2018)) without applying the notch filter to the new residual or estimating the payload dipoles again. The newly found residual force and torque are used as inputs to the wind algorithm in section 3 (Fig. 1) to find the new thermospheric wind. The sensitivity is expressed as the mean (μ) and standard deviation (σ) of the difference between the newly derived and the nominal wind. These values are calculated per wind direction (horizontal and vertical) and source data (forces F or

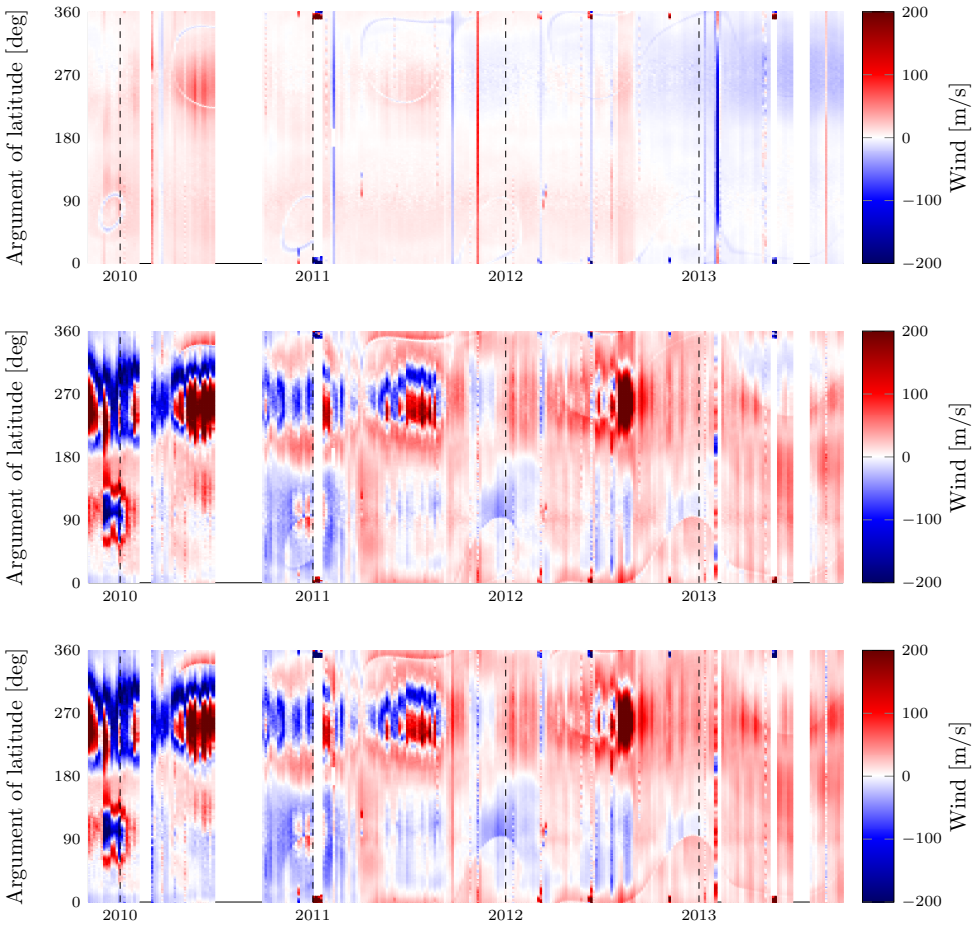

Figure 5: Vertical wind derived from forces (top) and torques (middle), and the difference between the two, for the full mission.

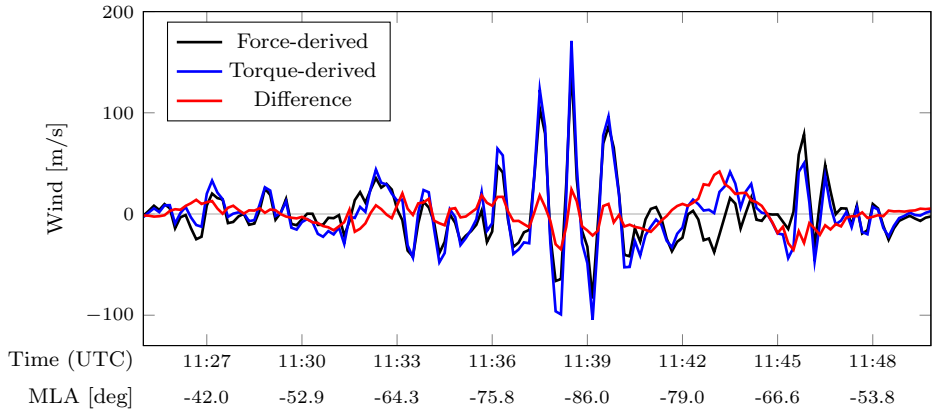

Figure 6: Times series of strong vertical wind peaks on 17 March 2013 over the South pole. Both force- and torque-derived wind are high-pass filtered to reveal their similarity above ten times the orbital frequency. Magnetic latitude (MLA) is added for reference.

torques T). Parameters that constitute a full 3×3 matrix (moment of inertia, magnetometer scale factor, control dipole scale factor, soft magnetic dipole) are only changed along the diagonal.

All measurements considered here are listed in Table 3. The uncertainty levels of the mass properties are taken from the numerical precision in the documentation. For the vertical acceleration we use the root mean square error of the fit in Fig. 3 instead of the standard deviation of the orbit-derived estimates. The uncertainty in angular acceleration is obtained from the bias estimates of Visser et al. (2018), even though we no longer use those accelerations, and our current error is likely smaller. The root mean square error of the fit in Fig. 3 of Visser et al. (2018) is used as the scale factor error of the magnetic field.

For the model parameter uncertainties in Table 4 we extensively use the root mean square error of linear fits, either presented in this paper or our previous work (Visser et al., 2018). Exceptions are the thrust offset and thrust level that were taken from documentation, and the aerodynamic parameters (accommodation coefficients, specular fraction, atmospheric and wall temperature, and flow speed) that were chosen arbitrarily. With flow speed we mean the magnitude of the velocity vector. Since this magnitude is kept constant in the cross-wind algorithm, this effectively reflects a constant along-track head-wind of 200 m/s.

Table 3: Sensitivity of force-derived ($_F$) and torque-derived ($_T$) cross-wind to measurement errors, in terms of the mean (μ) and standard deviation (σ) of the wind difference, evaluated for March 2013.

		Horizontal [m/s]		Vertical [m/s]	
Parameter	Value	$\mu_F \pm \sigma_F$	$\mu_T \pm \sigma_T$	$\mu_F \pm \sigma_F$	$\mu_T \pm \sigma_T$
CoM shift x [mm]	0.5[a]	(−)±(−)	0.10±0.19	(−)±(−)	−0.35±0.05
CoM shift y [mm]	0.5[a]	(−)±(−)	−0.00±0.00	(−)±(−)	−0.00±0.00
CoM shift z [mm]	0.5[a]	(−)±(−)	0.00±0.00	(−)±(−)	−0.00±0.00
Roll bias [”]	3[b]	−0.00±0.00	0.00±0.01	0.00±0.00	0.00±0.00
Pitch bias [”]	3[b]	−0.00±0.00	−0.00±0.00	−0.11±0.00	0.31±0.15
Yaw bias [”]	3[b]	0.11±0.00	0.11±0.00	−0.00±0.00	0.00±0.00
Inertia x [kgm^2]	0.05[a]	(−)±(−)	0.00±0.00	(−)±(−)	−0.00±0.00
Inertia y [kgm^2]	0.05[a]	(−)±(−)	−0.00±0.00	(−)±(−)	−0.00±0.00
Inertia z [kgm^2]	0.05[a]	(−)±(−)	0.00±0.01	(−)±(−)	0.00±0.00
Mass [kg]	0.0005[a]	−0.00±0.00	(−)±(−)	0.00±0.00	(−)±(−)
Lin. acc. x [nm/s^2]	0.3[c]	−0.00±0.01	(−)±(−)	0.00±0.00	(−)±(−)
Lin. acc. y [nm/s^2]	7[c]	−4.31±1.46	(−)±(−)	0.02±0.03	(−)±(−)
Lin. acc. z [nm/s^2]	3[e]	−0.01±0.02	(−)±(−)	−2.79±0.93	(−)±(−)
Ang. rate x [nrad/s]	10[b]	(−)±(−)	−0.05±0.02	(−)±(−)	0.00±0.00
Ang. rate y [nrad/s]	10[b]	(−)±(−)	0.00±0.00	(−)±(−)	−0.00±0.00
Ang. rate z [nrad/s]	10[b]	(−)±(−)	−0.00±0.00	(−)±(−)	0.00±0.00
Ang. acc. x [nrad/s^2]	4.2[e]	(−)±(−)	−0.01±0.01	(−)±(−)	−0.24±0.08
Ang. acc. y [nrad/s^2]	0.29[e]	(−)±(−)	0.00±0.02	(−)±(−)	−2.23±0.77
Ang. acc. z [nrad/s^2]	4[e]	(−)±(−)	18.89±6.46	(−)±(−)	−0.51±0.34
Magn. scale x [%]	0.1[e]	(−)±(−)	−0.00±0.03	(−)±(−)	−0.02±0.15
Magn. scale y [%]	0.1[e]	(−)±(−)	−0.00±0.06	(−)±(−)	0.00±0.01
Magn. scale z [%]	0.1[e]	(−)±(−)	0.00±0.00	(−)±(−)	−0.00±0.46

[a] Numerical precision in GOCE Mass Properties file.
[b] Stummer (2012).
[c] Visser and van den IJssel (2016).
[d] Kolkmeier et al. (2008).
[e] Root mean square error of fit, Visser et al. (2018) or this paper.
[f] Wallace et al. (2011).

Table 4: Sensitivity of force-derived ($_F$) and torque-derived ($_T$) cross-wind to model parameters, in terms of the mean (μ) and standard deviation (σ) of the wind difference, evaluated for March 2013.

		Horizontal [m/s]		Vertical [m/s]	
Parameter	Value	$\mu_F \pm \sigma_F$	$\mu_T \pm \sigma_T$	$\mu_F \pm \sigma_F$	$\mu_T \pm \sigma_T$
Thrust offset x [mm]	1.6[d]	(−)±(−)	−0.06±0.01	(−)±(−)	0.95±0.03
Thrust offset y [mm]	1.6[d]	(−)±(−)	17.03±0.55	(−)±(−)	−0.46±0.22
Thrust offset z [mm]	1.6[d]	(−)±(−)	−0.03±0.18	(−)±(−)	27.40±0.68
Thrust angle α [deg]	0.02[e]	0.00±0.01	−0.02±0.10	1.99±0.01	15.56±0.39
Thrust angle β [deg]	0.02[e]	−1.31±0.04	−9.67±0.33	0.00±0.01	0.26±0.13
Thrust level [%]	1[f]	0.55±1.27	0.69±1.20	−2.03±0.25	0.60±0.39
Dipole x [Am^2]	0.13[e]	(−)±(−)	−0.72±1.60	(−)±(−)	2.24±14.96
Dipole y [Am^2]	0.043[e]	(−)±(−)	−0.01±1.21	(−)±(−)	0.01±0.04
Dipole z [Am^2]	0.051[e]	(−)±(−)	−0.00±0.01	(−)±(−)	−0.02±2.33
Control dipole x [%]	0.96[e]	(−)±(−)	−0.32±1.07	(−)±(−)	0.91±10.12
Control dipole y [%]	1.93[e]	(−)±(−)	−0.16±0.52	(−)±(−)	0.00±0.02
Control dipole z [%]	1.72[e]	(−)±(−)	0.00±0.02	(−)±(−)	−0.22±2.57
Soft dipole x [Am^2/T]	1338[e]	(−)±(−)	−0.02±0.24	(−)±(−)	−0.04±1.87
Soft dipole y [Am^2/T]	1096[e]	(−)±(−)	0.02±0.20	(−)±(−)	0.00±0.01
Soft dipole z [Am^2/T]	683[e]	(−)±(−)	0.00±0.01	(−)±(−)	0.02±0.95
Accommodation [-]	0.6	12.48±34.77	−4.10±31.72	−1.73±4.25	2.15±2.15
Accommodation [-]	0.8	7.47±20.84	−2.37±18.87	−0.97±2.39	1.17±1.20
Accommodation [-]	1	−13.34±38.67	3.69±33.40	1.30±6.37	−1.55±1.70
Specular frac. [-]	0.01	−0.11±0.30	1.25±0.45	0.04±0.11	0.17±0.26
Specular frac. [-]	0.02	−0.21±0.60	2.50±0.90	0.08±0.21	0.34±0.52
Specular frac. [-]	0.03	−0.32±0.90	3.74±1.34	0.12±0.32	0.52±0.78
Atmospheric temp. [K]	200	−0.43±0.63	−1.26±1.49	0.03±0.13	0.70±0.63
Wall temp. [K]	200	0.47±1.29	−0.17±1.17	−0.06±0.15	0.07±0.07
Flow speed [m/s]	200	−3.04±2.76	−2.43±2.58	−0.19±0.29	0.28±0.60

[a] Numerical precision in GOCE Mass Properties file.
[b] Stummer (2012).
[c] Visser and van den IJssel (2016).
[d] Kolkmeier et al. (2008).
[e] Root mean square error of fit, Visser et al. (2018) or this paper.
[f] Wallace et al. (2011).

More than half of the parameters listed in Tables 3 and 4 affect only the torque-derived wind. On top of that the thrust angles produce significantly larger offsets in torque-derived wind than in their force-derived counterparts. This confirms our hypothesis that force modeling is less error-prone, and the wind derived from that is thus likely closer to the true wind. We discuss the four most prominent parameters in more detail below. Their effect on the wind data is plotted against magnetic latitude in Fig. 7.

First and foremost the thruster misalignment plays a central role. From Table 4 and Fig. 7 we conclude that thrust pitch causes almost purely an offset in vertical winds, and thrust yaw in horizontal winds. The large discrepancy in sensitivity of the two data sets makes this an ideal parameter to improve their consistency. Note that the mean and standard deviation in Table 4 are computed for an error of 0.02deg (the maximum root mean square error of the fits in Fig. 2), whereas a maximum error of 0.9deg is reported (Kolkmeier et al., 2008). For such values of thruster misalignment the wind offsets reach values in excess of 1000 m/s. An offset in the thrust application point has a similar effect on the torque-derived wind, but its maximum magnitude is much smaller.

Second the longitudinal component of the spacecraft magnetic dipole has a significant influence on the torque-derived wind. The vertical wind is affected the most, because of the large influence of magnetic torques on the pitch axis (Visser et al., 2018). The difference is the largest at the magnetic poles, due to the orientation of the magnetic field.

Third the energy accommodation coefficient is changed. Note that we choose a small change of only 0.03 to compare it to the specular fraction hereafter. The parameter has a strong influence on the horizontal wind. Comparing the trend in the nominal wind and the difference, we may conclude that the accommodation coefficient primarily scales the horizontal wind. This specific pattern was also observed by Dhadly et al. (2018) (see Fig. 2), who assumed it was a latitude-dependent offset. The vertical wind is less sensitive to the accommodation coefficient, but reveals an interesting trend. While the nominal force-derived wind decreases towards the poles, the torque-derived wind increases; at the same time the differences show the opposite trend. This suggests that lowering the accommodation coefficient may improve the consistency of the vertical wind. A future study will focus on the effect of accommodation on the consistency of estimated parameters and the GOCE wind data.

Finally the specular fraction of the particle–surface interaction is investi-

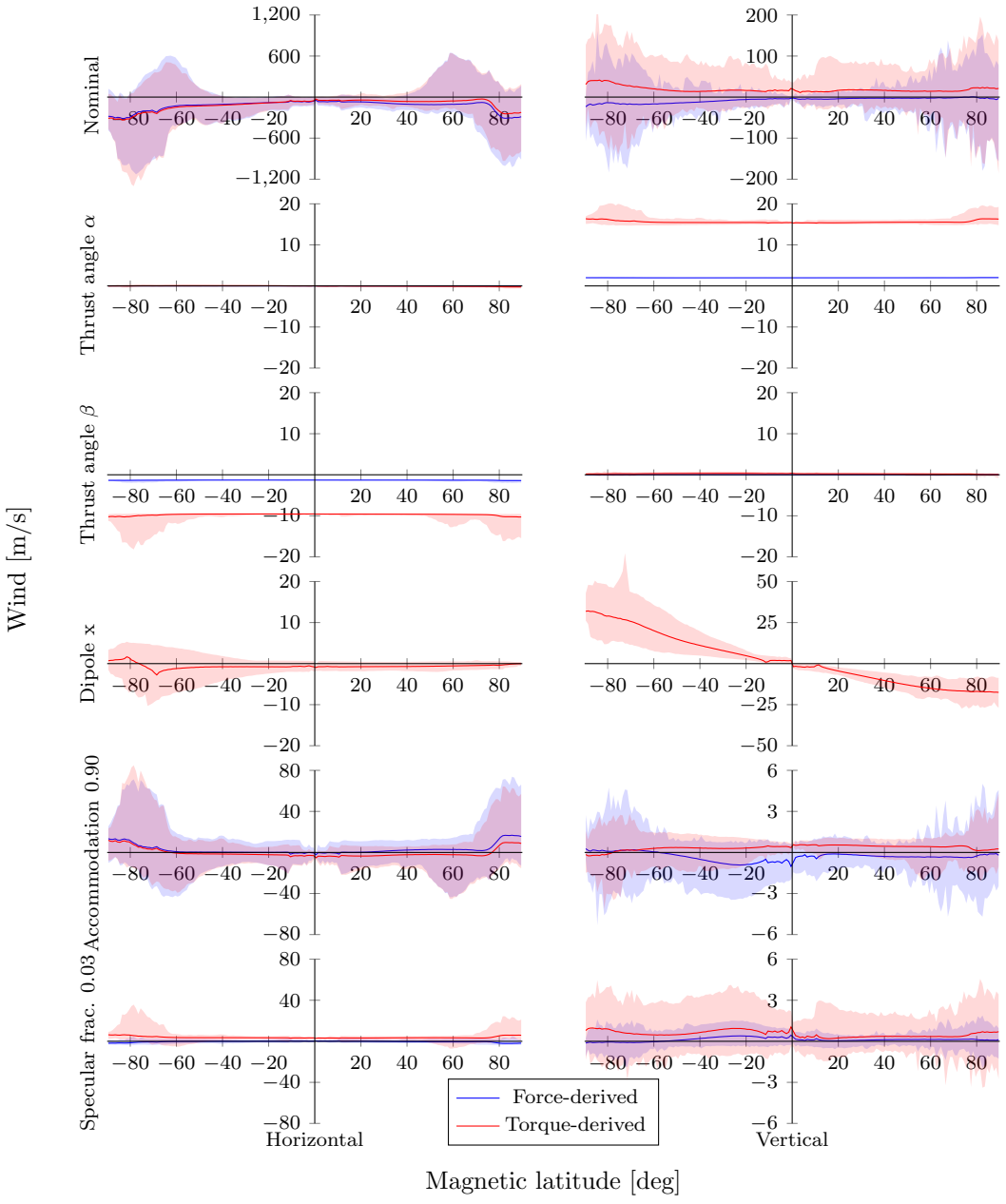

Figure 7: Horizontal (left) and vertical wind difference from nominal due to a selection of model parameters from Table 4, in terms of min-mean-max over one degree magnetic latitude bins for March 2013. Note the different limits on the vertical axes.

gated. The change from 0 to 3% causes a smaller change in horizontal wind than a similar change in energy accommodation. Contrary to the latter, the specular fraction seems to mostly affect the torque-derived wind. The overall trend of the difference is similar to that of the nominal wind.

6. Conclusion

Comparing the cross-wind data sets presented in this paper, taking into account the required effort to arrive at the current model fidelity, we conclude that although it is possible to obtain cross-wind from angular acceleration measurements, it is highly impractical. In the specific case of GOCE the most problematic model parameter is the thruster misalignment. The extreme sensitivity to these angles forces us to use the force-derived wind measurements to tune the torque-derived ones. This fact implies that satellites that use continuous thrusting are not suitable for deriving wind purely from attitude motion. More generally for low-Earth-orbiting accelerometer missions currently in use, the knowledge of the magnetic properties of the satellite is likely insufficient to do without the dipole estimation procedure of Visser et al. (2018). Although these estimates have greatly improved the result, we have strong indications that the remaining differences between the two wind data sets are still strongly linked to the Earth's magnetic field. This implies that we still lack knowledge of the magnetic and electronic properties of GOCE. Note that attempts to obtain magnetic properties as a function of large internal currents have failed for GOCE in the past (Visser et al., 2018). Later attempts to explain the difference by satellite charging, or static charges in the ion engine, have failed because the required charges were several orders of magnitude higher than anticipated. We conclude that if accurate data is to be obtained from the attitude motion of future satellites, a complete magnetic dipole budget is required, including current loops and electrically charged elements.

The difficulties described above mostly pertain to the lower frequencies. These are also the frequencies at which the estimation of magnetic dipoles, thruster misalignment angles, and acceleration bias have their primary effect. Horizontal wind errors are dominated by a once-per-orbit signal, and at frequencies above ten times orbital frequency the force- and torque-derived vertical cross-winds show a strong correlation. We may conclude that the force-derived wind is thus internally validated at frequencies above ten times

orbital frequency by the torque-derived data. At the same time the mean vertical wind cannot be determined from the GOCE accelerometer data alone.

This form of internal validation of the force-derived wind is also the true value of simultaneous wind observations from linear and angular accelerations. The total set of estimated model parameters provides us with the opportunity to test the consistency of wind measurements without the need for other measurement sources. Instead of tuning aerodynamic model parameters (such as the energy accommodation coefficient) to match other models and observations, we may look for parameters that provide the most consistent estimates of magnetic, thruster, and calibration parameters. In this respect we have strong indications that the accommodation coefficient needs to be lowered from its current value of 0.93.

A similar simultaneous estimation of the density using GOCE linear and angular acceleration data is impossible. Due to the satellite's geometric design the aerodynamic response in roll is too small to be used in the presented algorithm, reducing the number of independent measurements to five. Horizontal wind can be obtained from the lateral force or the yaw moment, vertical wind from the vertical force or the pitch moment, neutral density only from the longitudinal force. If a simultaneous density estimation is desired in a future mission, the paddlewheel concept could be applied to the GOCE design by rotating the fins accordingly.

References

Bruinsma, S., Tamagnan, D., Biancale, R., 2004. Atmospheric densities derived from CHAMP/STAR accelerometer observations. Planetary and Space Science 52, 297–312.

Cheng, M., Tapley, B. D., Bettadpur, S., Ries, J. C., 2008. Determination of thermospheric winds from GRACE accelerometer data. In: Advances in the Astronautical Sciences. Vol. 130. pp. 1181–1192.

Dhadly, M., Emmert, J., Drob, D., Conde, M., Doornbos, E., Shepherd, G., Makela, J., Wu, Q., Niciejewski, R., Ridley, A., February 2017. Seasonal dependence of northern high-latitude upper thermospheric winds: A quiet time climatological study based on ground-based and space-based measurements. Journal of Geophysical Research: Space Physics 122 (2), 2619–2644.

Dhadly, M. S., Emmert, J. T., Drob, D. P., Conde, M. G., Doornbos, E. N., Shepherd, G. G., Makela, J. J., Wu, Q., Nieciejewski, R. J., Ridley, A. J., January 2018. Seasonal dependence of geomagnetic active-time northern high-latitude upper thermospheric winds. Journal of Geophysical Research: Space Physics 123 (1), 739–754.

Doornbos, E., March 2011. Thermospheric Density and Wind Determination from Satellite Dynamics. Ph.D. thesis, Delft University of Technology.

Doornbos, E., van den IJssel, J., Lühr, H., Förster, M., Koppenwallner, G., July-August 2010. Neutral Density and Crosswind Determination from Arbitrarily Oriented Multiaxis Accelerometers on Satellites. Journal of Spacecraft and Rockets 47 (4), 580–589.

Falin, J. L., Barlier, F., Kockarts, G., 1981. Densities from the CACTUS accelerometer as an external test of the validity of the thermospheric models. Advances in Space Research 1 (12), 221–225.

GOCE Flight Control Team (HSO-OEG), Feb. 2014. GOCE End-of-Mission Operations Report. Tech. Rep. GO-RP-ESC-FS-6268.

Innis, J. L., Conde, M., August 2002. High-latitude thermospheric vertical wind activity from Dynamics Explorer 2 Wind and Temperature Spectrometer observations: Indications of a source region for polar cap gravity waves. Journal of Geophysical Research 107 (A8, 1172).

Kolkmeier, A., Präger, G., Möller, P., Strandberg, T., Kempkens, K., Stark, J., Gessler, L., Hienerwadel, K. O., April 2008. GOCE - DFAC Interface Control Document. Tech. Rep. GO-IC-ASG-0005_12, EADS Astrium.

March, G., Doornbos, E. N., Visser, P. N. A. M., July 2018. High-fidelity geometry models for improving the consistency of CHAMP, GRACE, GOCE, and Swarm themrmospheric density data sets. Advances in Space Research ? (?), ?

Mehta, P. M., Walker, A. C., Sutton, E. K., Godinez, H. C., 2017. New density estimates derived using accelerometers on board the CHAMP and GRACE satellites. Space Weather 15 (4), 558–576.

Moe, K., 1966. Absolute atmospheric densities determined from the spin and orbital decays of explorer VI. Planetary and Space Science 14 (11), 1065–1075.

Pilinski, M., Moe, K., Palo, S., Argrow, B., July 2011. Measuring absolute thermospheric densities and accommodation coefficients using paddlewheel satellites: past findings, present uses, and future mission concepts. Journal of the Astronautical Sciences 58 (3), 531–549.

Siemes, C., January 2018. Improving GOCE cross-track gravity gradients. Journal of Geodesy 92 (1), 33–45.

Siemes, C., De Teixeira Da Encarnao, J., Doornbos, E., Van Den IJssel, J., Kraus, J., Peret, R., Grunwaldt, L., Apelbaum, G., Flury, J., Holmdahl Olsen, P. E., 2016. Swarm accelerometer data processing from raw accelerations to thermospheric neutral densities 2. aeronomy swarm science results after two years in space. Earth, Planets and Space 68 (1), 92.

Smith, R. W., 1998. Vertical winds: a tutorial. Journal of Atmospheric and Solar-Terrestrial Physics 60, 1425–1434.

Stummer, C., October 2012. Gradiometer Data Processing and Analysis. Ph.D. thesis, Institut für Astronomische und Physikalische Geodäsie.

Sutton, E. K., Forbes, J. M., Nerem, R. S., 2005. Global thermospheric neutral density and wind response to the severe 2003 geomagnetic storms from CHAMP accelerometer data. Journal of Geophysical Research: Space Physics 110 (A9).

Virgili-Llop, J., Roberts, P., Hao, Z., March 2018. Using the attitude response of aerostable spacecraft to measure thermospheric wind. CEAS Space Journal 10 (1), 101–113.

Visser, P., van den IJssel, J., 2016. Calibration and validation of individual GOCE accelerometers by precise orbit determination. Journal of Geodesy 90, 1–13.

Visser, T., Doornbos, E., de Visser, C., Visser, P., Fritsche, B., September 2018. Torque model verification for the goce satellite. Advances in Space Research 1 (1), 1–23.

Wallace, N., Jameson, P., Saunders, C., Fehringer, M., Edwards, C., Floberghagen, R., September 11-15 2011. The GOCE ion-propulsion assembly - lessons learnt from the first 22 months of flight operations. In: 32nd International Electric Propulsion Conference, Wiesbaden, Germany.